RESEARCH ARTICLE

Thermal, Dynamic Mechanical, Mechanical and Flammability Properties of Halloysite Nanotubes Filled Polyamide 11 Nanocomposites

Nur Najma Athirah Azahari[a,*], Hazleen Anuar[a], Azman Hassan[b], Mohammed Jawaid[c], Zahurin Halim[a], Sani Amril Samsudin[d]

[a]Department of Manufacturing and Materials Engineering, Kulliyyah of Engineering, International Islamic University Malaysia, 53100 Gombak, Kuala Lumpur, Malaysia; [b]School of Bioprocess and Polymer Engineering, Faculty of Chemical and Energy Engineering, Universiti Teknologi Malaysia, 81310 UTM Johor Bahru, Johor, Malaysia; [c]Department of Biocomposite Technology Lab, Institute of Tropical Forestry and Forest Product, Universiti Putra Malaysia, 43400 Serdang, Selangor, Malaysia; [d]School of Chemical Engineering and Energy Engineering, Faculty of Engineering, 81310 UTM Johor Bahru, Johor, Malaysia

*For correspondence:
najmatyraazahari@gmail.com

Abstract The effects of various filler contents on the thermal, dynamic mechanical, mechanical, as well as flammability properties of halloysite nanotubes (HNTs) filler and polyamide 11 (PA 11) matrixes are investigated in this research. The nanocomposites were made out of 100 phr of PA 11 and three distinct HNTs loadings of 2, 4, and 6 phr each. PA 11 nanocomposites without HNTs filler was used as the reference sample. To melt-compound the nanocomposites, a twin-screw extruder was used, and the specimen for testing was then injected using an injection mold. SEM, TGA, DSC, FTIR, DMA, tensile, flexural, impact, and UL-94 flammability tests were conducted on the nanocomposites. Incorporation of 4 phr HNTs into the nanocomposites resulted in the highest tensile and flexural strength. Maximum improvement in the DMA, Young's and flexural modulus was achieved at 6 phr HNTs content. The elongation at break and TGA resulted the highest increase at 2 phr HNTs content. However, the impact strength decreased with increasing HNTs content. Scanning electron microscopy revealed the ductility of the nanocomposites with increased HNTs content up to 4 phr. The DSC showed a steady increase in melting temperature (T_m) as HNTs content increased up to 4 phr, while the crystallization temperature (T_c) remained unchanged. TGA of PA 11/HNTs nanocomposites showed high thermal stability at 2 phr HNTs content. However, on further addition of HNTs up to 6 phr, thermal stability of the nanocomposites decreased due to the excess amount of HNTs. All the nanocomposites passed the horizontal and vertical UL-94 test with HB and V-2 grade. PA 11/4HNTs nanocomposite has the highest tensile strength, flexural strength compared to other PA 11/HNTs nanocomposites. PA 11/4HNTs nanocomposite can be suggested as an optimum formulation with balanced mechanical properties in terms of toughness.

Keywords: Polyamide, Halloysite nanotubes, nanocomposites, mechanical properties, flammability properties.

Introduction

Compared to other extensively used polyamides, Polyamide 11 (PA 11) has the benefit of being bio-based and less hydrophilic. It is a type of semi-crystalline [1] polymer derived from castor oil that is widely employed in industries ranging from offshore to automotive as an engineering polymer. PA 11 has many

benefits, including exceptional impact strength, good chemical resistance, low water absorption, stress cracking, ageing, and abrasion resistance, as well as the ability to accept high filler loading, besides low coefficient of friction [2]. However, PA 11 is not without disadvantages which include low stiffness and low heat resistance.

The addition of a slight amount of nanofillers to multifunctional polymer systems has gained a lot of attention [3]. The increased surface area of nanofillers and favorable matrix/nanofiller interactions, which led to improved characteristics when compared to pure polymers, have sparked a lot of interest in polymer nanocomposites [4]. Halloysite nanotubes (HNTs) are a type of nanofiller [5] that come in a variety of forms and sizes. HNTs are aluminosilicate clay minerals with the chemical formula $Al_2Si_2O_5(OH)_4.nH_2O$ [6], which exist naturally [7]. They contain oxygen, silicon, aluminium, and hydrogen. Compared to other nanotubes, HNTs are environmentally friendly nanotubes using low-cost materials. HNTs are excellent at improving thermoplastics' thermal stability, mechanical, and flame-retardant qualities, besides easy to produce [8]. Using HNTs to improve flame retardant is a novel idea because it does not reduce mechanical strength [9].

Many studies have found that adding HNTs to PA 11 improves the microstructure and final properties of the material [10]. According to research, tensile strength, young's modulus, and elongation at break have all improved in PA 11/HNTs nanocomposites. Francisco et al. [11] studied the mechanical properties of polyamide 11 nanocomposites loaded with halloysite nanotubes, as well as their connection. The HNTs were inserted into a PA 11 matrix via melt extrusion with a twin-screw extruder and an injection molding machine, with 2, 6, and 10 wt.% HNTs loading. HNTs improve flexural strength, flexural modulus of elasticity, yield stress, and tensile modulus of elasticity, but decrease tensile strength significantly, according to researchers. Sahnoune et al. [12] studied the tribological and mechanical properties of polyamide-11/halloysite nanotube nanocomposites produced by melt-compounding with 1, 3, and 5 wt.% raw Algerian and commercial HNTs loading. According to the researchers, adding HNTs to PA 11 appears to be an efficient technique for generating nanocomposite materials with increased mechanical and tribological performance. Raw Algerian HNTs produced better results as compared to commercial HNTs. Prashantha et al. [10] investigated the thermal, rheological, optical, dielectric, and mechanical characteristics of polyamide-11/Halloysite nanocomposites produced by melt extrusion with 2, 4, and 6 wt.% HNTs concentration using a master batch dilution procedure. They discovered that incorporating HNTs into nanocomposites increased the materials' mechanical and thermal stability. Sahnoune et al. [13] also investigated the effects of gamma irradiation on the structural, thermal, and mechanical properties of polyamide-11/halloysite nanotube nanocomposites generated by melt-compounding with 3 wt.% HNTs content. They discovered that crosslinking occurs at low irradiation levels, while chain scission occurs at larger doses, and that HNTs act as a barrier to the effects of gamma irradiation. It was determined that the ideal irradiation dose for thermal and mechanical properties corresponded to the dose for maximum gel formation. Another study was carried out by Bugatti et al. [1] on antimicrobial membranes consisting of bio-based PA 11 and HNTs loaded with lysozyme synthesized by an electro spinning process with HNTs values of 1.0, 2.5 and 5.0 wt.%. They found that increasing the amount of filler increased mechanical properties and that PA 11 and lysozyme molecules interacted nicely.

Melt-blending with a twin-screw extruder and injection molding with varied HNTs loadings of 2, 4, and 6 phr were used to make the PA 11/HNTs nanocomposites in this study. The main goal of this study was to investigate the effect of HNTs loading on morphology using scanning electron microscopy (SEM), thermal properties using thermogravimetric analysis (TGA) and differential scanning calorimetry (DSC), viscoelastic properties using dynamic mechanical analysis (DMA), Fourier transform infrared spectroscopy (FTIR), mechanical properties using tensile, flexural and Charpy impact testing, and flammability properties using UL-94 standard flammability of the nanocomposites. Although many researchers have worked on PA 11/HNTs nanocomposites, there has been very little research on their dynamic mechanical characterization and flammability features. One of the more essential criteria for developing the ultimate use of products is the material's flammability and viscoelasticity.

Materials and Methods

Polyamide 11 brand Rilsan® BMN G8 TLDA resin with a melting temperature of 190 °C was purchased from Arkema Inc., Lacq, France.

Halloysite nanotubes brand Dragonite organoclay with basic composition of HNTs (wt.%): $Al_2O_3.2SiO_2.2H_2O$, 95; SiO_2. The specific gravity of HNTs is 2.53. HNTs with a diameter of 80 nm, a length of 1.2 cm and a density of 2.5 g/cm^3 were purchased from Applied Minerals in New York.

Preparation of Nanocomposites

PA 11 granules and HNTs powder were dried in a vacuum oven at 80 ℃ for 8 hours to remove moisture. PA 11 matrix could easily absorb moisture in the past, causing it to go through drying procedures. 100 phr PA 11 pellets packed with 2, 4, and 6 phr HNTs powder were used to make the nanocomposites. **Table 1** shows the designated name of the formulation. PA 11 and HNTs were manually combined in the container before being fed into the hopper of a Brabender Plastic Corder, PL 2000, counter-rotating twin-screw extruder. Heating temperatures of 220 ℃ (zone 1), 225 ℃ (zone 2), 230 ℃ (zone 3) and 235 ℃ (die) were selected as the extrusion temperatures. The rotational speed of the screw was adjusted at 60 revolutions per minutes. Extruded materials were cooled before being cut into pellets using a laboratory scale pelletizer. The pellets were dried in a vacuum oven at 80 ℃ for 5 hours [14] before being injected into test specimen using the JSW 80 Ton injection molding machine. The temperature was held between 220-235 ℃ from the hopper to the nozzle, while a water-cooling system was used to keep the mold temperature 25 ℃. Injection flow was set at 50 cm^3s^{-1} while, the screw rotation speed and holding pressure were set at 300 bar and 100 rpm, respectively.

Table 1. Composition of the PA 11/HNTs nanocomposites.

Material Designation	PA 11 (phr)	HNTs (phr)
PA 11	100	0
PA 11/2HNTs	100	2
PA 11/4HNTs	100	4
PA 11/6HNTs	100	6

Characterization of Nanocomposites

Scanning Electron Microscopy

The post-tensile fracture surfaces of the nanocomposites were studied using a scanning electron microscope (SEM) JSM 5600. Before being placed in the specimen chamber, samples were sputter coated with Palladium to give them conductive properties. The images were captured using various magnification settings at an accelerated voltage of 8.0kV.

Thermogravimetric Analysis

The sample's thermal stability was determined using a Perkin Elmer thermogravimetric analyzer (TGA 4000). Four samples around 8 to 10 mg were scorched from 20 to 600 ℃ at a rate of 10 ℃/min in a nitrogen environment to study thermal degradation behavior. The nitrogen flow rate was 20 milliliters per minute. From derivative thermogravimetric (DTG) data, the temperature at 10% weight loss (T_{10}), the temperature of maximum degradation rate (T_{max}), the final degradation temperature showed by the end temperature (T_{end}), and residual weight percent recorded at 600 ℃ were also obtained [15].

Differential Scanning Calorimetry

The differential scanning calorimetry (DSC) measurements were performed with a Mettler Toledo DSC apparatus in a nitrogen environment with a gas flow rate of 40 mL/min and a heating rate of 10 ℃/min [16]. Temperatures ranging from 30 to 200 ℃ were used to create the thermogram. The temperature was decreased to 20 ℃ at 10 ℃/min to erase the thermal history of the PA 11 polymer and analyze the recrystallization of PA 11/HNTs nanocomposites [17]. The samples were heated to 220 ℃ at a rate of 10 ℃/min in the second scan [18]. The crystallization temperature (T_c), melting temperature (T_m) and crystallization enthalpy (ΔH_c) of virgin PA 11 polymer and PA 11/HNTs nanocomposites were measured [10]. The degree of crystallinity (X_c) of the nanocomposites was calculated using (Eq. 1):

$$X_c = \frac{\Delta H_m}{\Delta H_m^\circ} \times 100 \qquad\qquad (Eq.1)$$

Where ΔH_m is the melting enthalpy and ΔH°_m is the enthalpy of melting of the 100% crystalline polymer (ΔH°_c = 206 Jg^{-1}) [10; 19].

Fourier-Transform Infrared Spectroscopy Analysis

Fourier transform infrared spectroscopy (FTIR) was performed using a Perkin Elmer 1600 infrared spectrometer [19]. Nicolet's AVATAR 360 was used to measuring the materials' IR spectra in 32 scans

with a resolution of 4 cm^{-1} between 4000-300 cm^{-1} range. FTIR was used to explore the chemical interactions between PA 11 matrix and HNTs filler.

Dynamic Mechanical Analysis

The viscoelastic behavior in tension was investigated using dynamic mechanical analysis (DMA) according to ASTM D7028, using a Perkin Elmer DMA device and a heating rate of 3 ℃/min from 20 to 120 ℃ [20]. A three-point bending fixture was used at a frequency of 1 Hz. The rectangular DMA specimens were cut from injection molded rectangular bar samples having sample dimensions of 60 mm ✕ 13 mm ✕ 3 mm in size.

Tensile Testing

The tensile test is described as the force needed to break a specimen as it stretches and elongates until it breaks. Tensile tests were carried out using a Shimadzu Autograph AGS-X series universal material testing machine with a crossed speed of 50 mm/min and a 50 kN load cell [21], in accordance with ASTM D638. Samples with a gauge length of 25 mm were made and tested at 25 ± 2 ℃ and 50 ± 5% relative humidity to evaluate the tensile strength, tensile modulus, and tensile strain of the nanocomposites. The averages of five samples of each formulation were recorded.

Flexural Testing

The flexural test was performed using an Instron Universal Testing Machine that follows ASTM D790, a three-point bending system approach. A support span of 100 mm and a crosshead speed of 3.0 mm/min were used to examine the specimens. The flexural test produced flexural strength and flexural modulus results [22]. The averages of five samples of each formulation were presented.

Impact Testing

The specimens with varying proportions were subjected to a V-notched Charpy impact test using a pendulum-type impact tester, as per ASTM D256. Prior to the test, all the specimens were nicked in the middle using an automatic notching machine with a 0.25 mm notch depth. After measuring the specimens, they are supported on both ends by an anvil and struck by a pendulum on the opposite face of the notch. The amount of energy absorbed in breaking the test piece was calculated, yielding a notch toughness estimate for the test material. The pendulum swung across the table during the test, where the height of the swing indicates the amount of energy absorbed in shattering the specimen. Each formulation was tested five times, and the average was calculated.

UL-94 Flammability testing

UL-94 procedures were used to conduct the flame tests. On 125 ✕ 13 ✕ 3 mm sample positioned horizontally along the length and at 45º angle across the width, a standard UL-94 HB conforming the horizontal combustion test was carried out (**Figure 1**). A blue flame was applied at a distance of 25 mm, 45º to the horizontal, for 30 seconds. The flame was then removed, and the time to extinguish the fire, and the rate of burning were recorded [23]. On the same materials, UL-94 VB suggestive vertical burn tests were performed. A vertical blue flame was sprayed 25 mm from the base of a vertically mounted 125 ✕ 13 ✕ 3 mm specimen for 10 seconds (**Error! Reference source not found.**). The flame was reapplied for another 10 seconds after the sample vanished. Specimens that died in less than 10 seconds were given a V-0 rating. Specimens that extinguished without dripping before 30 seconds were given a V-1 rating [23], whereas those that extinguished with dipping were given a V-2 grade.
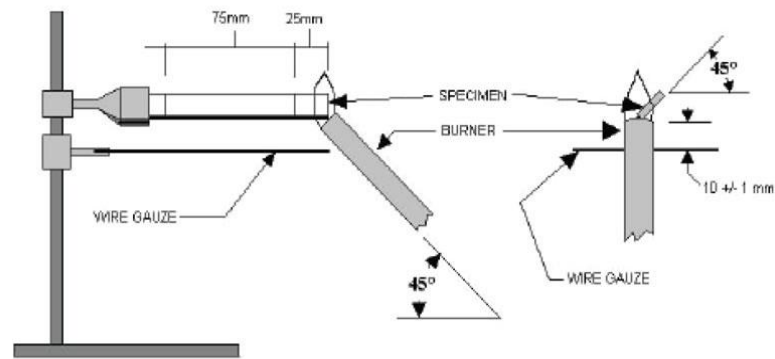
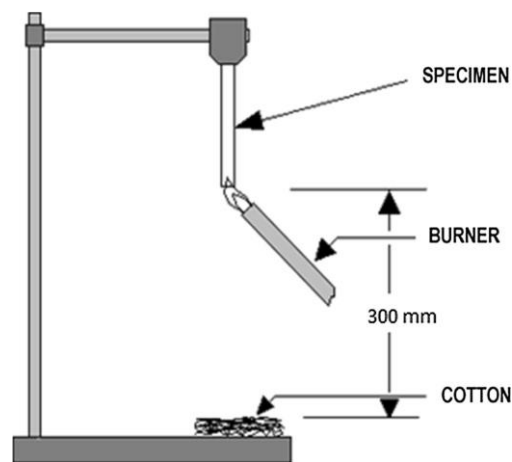**Figure 1.** Horizontal flammability tests based on UL-94 standards

Figure 2. Vertical flammability tests based on UL-94 standards

Results and Discussion

Nanotubes Dispersion
Scanning Electron Microscopy (SEM)

The scanning electron microscope was used to conduct the morphological investigations [13]. This method is commonly used in the material surface analysis. The scanning electron microscope was used to examine the morphologies and properties of the pure PA 11 polymer and the PA 11 containing varying amounts of HNTs in the ranges of 2, 4 and 6 phr, as shown in **Figure 3** (a), (b), (c), and (d). **Figure 3** (a) depicts the SEM features of the pure PA 11 matrix, which reveals a clear ductile fracture with a smooth surface and no HNTs particles. This finding is in line with the Wu research report [24], which found that many ligands are present on a fractural surface of pristine PA 11, accounting for the substance's ductility.

Figure 3 (b) shows the homogeneous and uniform HNTs dispersal in the PA 11 matrix at 2 phr, with most of the nanotube scattered at the nanoscale. Figure 3 (c) depicts that the HNTs are widely distributed throughout the PA 11 cracked surface at 4 phr, resulting in an increase in the tensile strength of PA 11 containing HNTs nanocomposites, as illustrated in Figure 12. This shows that HNTs dispersed in the PA 11 matrix function as reinforcement preventing the crack from propagating and improving the ductility of the nanocomposites. These findings are consistent with those of Sahnoune [13], who used SEM to confirm the nanocomposite shape of neat PA 11 and PA 11 filled with 3 wt.% HNTs nanocomposites. It can be seen as tiny aggregates, comparable to the micronic particles produced by the HNTs comminution process, according to the researchers. To generate a nanocomposite, HNTs are uniformly

and individually disseminated in the nano-range in the PA 11 matrix.

The tensile and flexural strength of the nanocomposites increase with the addition of HNTs, however, the tensile and flexural strength nanocomposites decrease as more HNTs are added. These findings are also consistent with Sharif et al., which mentioned the tensile strength of the material decreases as more HNTs are added into the nanocomposites [25]. The substantial agglomeration of HNTs in the PA 11 matrix, as observed in the SEM micrograph in Figure 3 (d), may create a separation of HNTs aggregates and PA 11 at the interface, which decreases the stress transfer of individual HNTs from PA 11. As shown in Figure 12 for a nanocomposites sample of 6 phr HNTs, this considerable aggregation of HNTs can eventually lead to voids at the PA 11 containing HNTs interface, a drop in the aspect ratio of HNTs, and a significant loss in the tensile strength of PA 11.
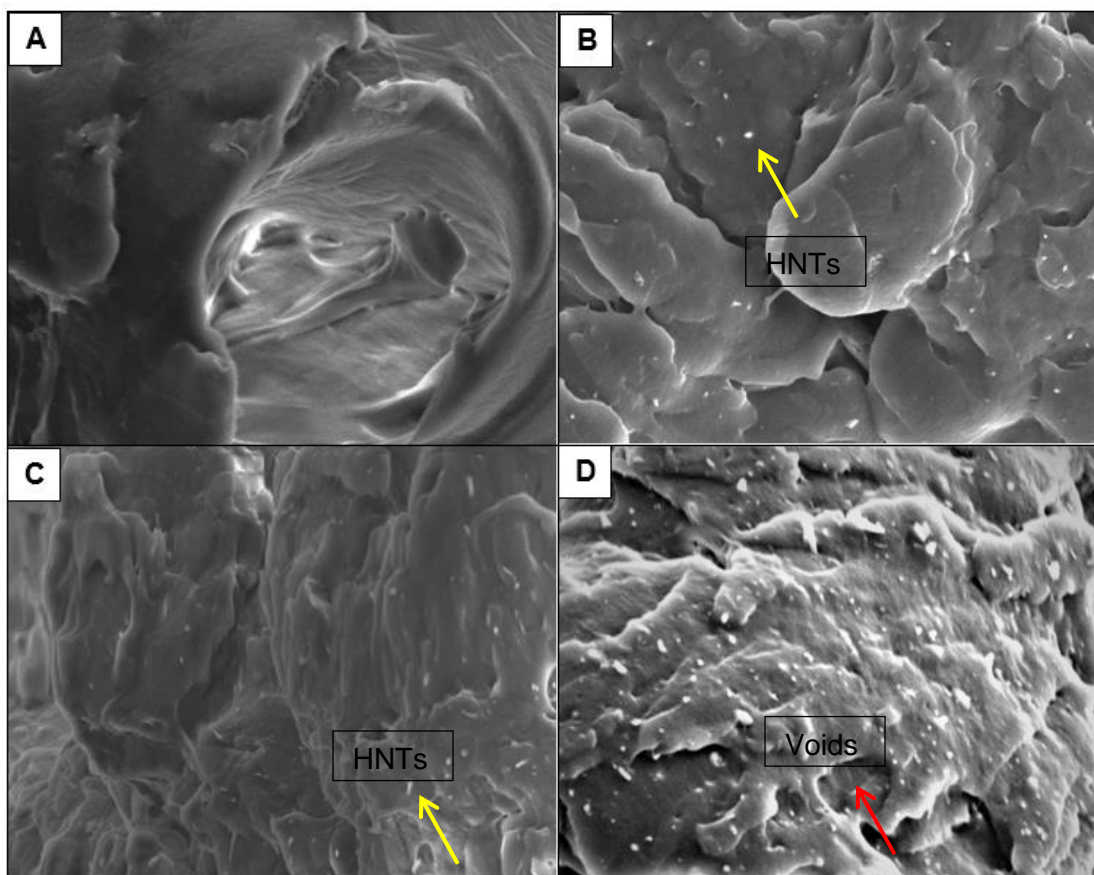

Figure 3. SEM micrographs of (a) pure PA 11 nanocomposites, (b) PA 11/2HNTs nanocomposites, (c) PA 11/4HNTs nanocomposites and (d) PA 11/6HNTs nanocomposites.

Thermal properties
Thermogravimetric Analysis (TGA)

Thermal properties of PA 11/HNTs nanocomposites were investigated by thermogravimetry analysis (TGA), compared with pure PA 11. The TGA was used to provide information about the nature and extent degradation of the polymeric materials as well as improvement in the thermal characteristics of these nanocomposites with addition of HNTs as nanofiller. Figure 4 and Figure 5 show the TGA and DTG curves for the PA 11 containing varying amounts of HNTs nanocomposites sample in the nitrogen atmosphere. Table 2 summaries the details.

When compared to pure PA 11 matrix, the TGA thermogram shows that PA 11 matrix with HNTs as filler yielded a significant change in an increase in all thermal properties, including temperature at 10% weight loss (T_{10}), maximum rate degradation temperature (T_{max}) and final degradation temperature showed by the end temperature (T_{end}) [26]. The T_{10} of pure PA 11 occurs at around 428.0 ℃, and it

decomposes entirely at 486.0 ℃, with no residue remaining. The presence of HNTs boosted the thermal stability of the nanocomposites, as seen in Table 2. With a higher temperature of 437.2 ℃, PA 11/2HNTs nanocomposites were the most thermally stable, as shown in Table 2. The temperature at 10% weight loss, the maximum rate of degradation temperature, and the final degradation temperature were all greater at PA 11/2HNTs composition than pure PA 11 [27].

However, increasing the number of HNTs in PA 11/4HNTs and PA 11/6HNTs nanocomposites reduces their thermal stability. Table 1 shows that as the HNTs content increased from 2 to 6 phr, the temperature at 10% weight loss decreased from 437.2 ℃ to 435.3 ℃ and 434.4 ℃, the temperature at the maximum rate of degradation decreased from 466.9 ℃ to 464.1 ℃ and 463.3 ℃ and the final degradation temperature decreased from 495.1 ℃ to 488.9 ℃ and 487.2 ℃, respectively. With increased filler addition, there was an increase in residue [28]. Because of the gradual increase of polymer chain mobility, the presence and effectiveness of HNTs as a nanofiller could be linked to an increase in thermal stability [29].

Table 2. Thermal degradation temperature of pure PA 11 and all PA 11 nanocomposites containing varying amounts of HNTs obtained from TGA and DTG thermogram.

Samples	T_{ON}[a] (℃)	T_{max}[b] (℃)	T_{OFF}[c] (℃)	Residue[d] (%)
PA 11	428.0	460.8	486.0	0
PA 11/2HNTs	437.2	466.9	495.1	0
PA 11/4HNTs	435.3	464.1	488.9	4.63
PA 11/6HNTs	434.3	463.3	487.2	4.71

[a]The temperature at 10% weight loss, [b]The maximum degradation temperature, [c]The final degradation temperature, [d]The amount of residue at 600 ℃
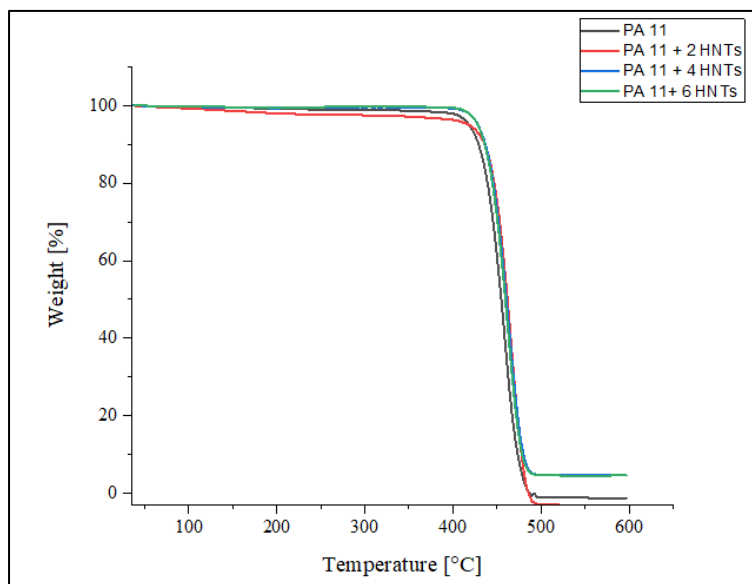

Figure 4. TGA thermogram of pure PA 11 and all PA 11 nanocomposites containing varying amounts of HNTs.
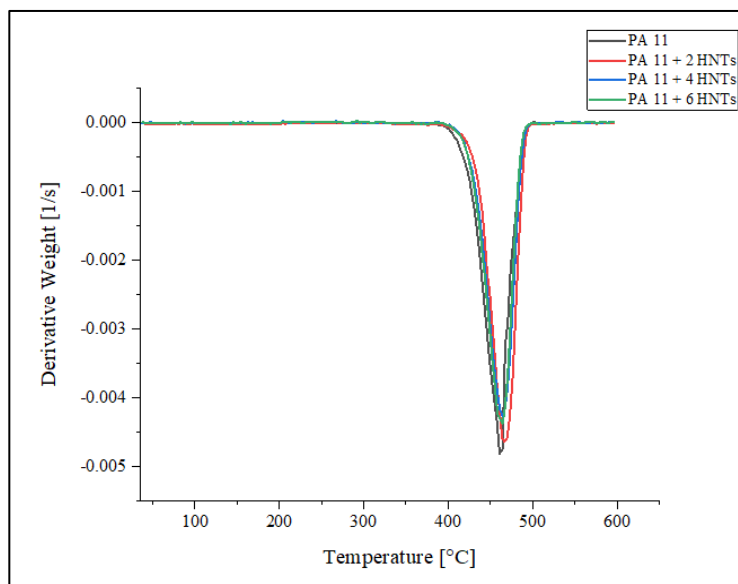
Figure 5. DTG thermogram of pure PA 11 and all PA 11 nanocomposites containing varying amounts of HNTs.

Table 3. Thermal characteristics of pure PA 11 and all PA 11 nanocomposites containing varying amounts of HNTs obtained from the DSC thermogram

Samples	Crystallization Temperature, T_c (℃)	Melting Temperature, T_m (℃)	Degree of Crystallinity, X_c (%)
PA 11	164.1	193.5	18.30
PA 11/2HNTs	165.1	193.9	19.17
PA 11/4HNTs	165.5	195.7	20.92
PA 11/6HNTs	165.3	194.7	19.22

Differential Scanning Calorimetry (DSC)

The amount of energy absorbed or released by the pure PA 11 and PA 11 containing varying amounts of HNTs nanocomposites when heated, cooled or held at a constant temperature was measured by DSC. Pure PA 11 is a semi-crystalline polymer whose thermal properties are determined by its crystallinity behavior, as measured by the crystallization temperature (T_c), melting temperature (T_m), and the degree of crystallinity (X_c). T_c is the crystallization point, which is the temperature at which a polymer crystallizes when heated or cooled and T_m stands for the melting point, which is the temperature at which a crystalline polymer melts. Aside from that, knowing the X_c, which is the degree of long-range order in a material that affects its qualities, is essential to comprehend the processability of PA 11 containing varying amounts of HNTs nanocomposites.

The first heating and cooling thermograms of pure PA 11 and PA 11 containing varying amounts of HNTs nanocomposites [30] are displayed in Figure 6 and Figure 7. The crystallization temperature (T_c), melting temperature (T_m), and degree of crystallinity (X_c) are summarized in Table 3. T_c was 164.1 ℃, T_m was 193.5 ℃, and X_c was 18.30% in the pure PA 11. Compared to the pure PA 11 matrix, there were substantial variations in crystallization temperature and the melting temperature of the nanocomposite with the presence of HNTs contents. This demonstrates that the addition of HNTs affects the nanocomposites' phase structure because nanofillers, which are frequently used in semi-crystalline thermoplastic elastomers, act as potent crystallization nucleating agents [31].

When compared to pure PA 11, it can also be noted that the X_c has also improved with the addition of HNTs. Well-dispersed HNTs have been shown to operate as nucleating agents, increasing semi-crystalline polymer crystallization rates and crystallinity [32; 33]. Including HNTs raised the T_m, T_c, and X_c,

according to Prashantha [10].

However, because of the production of tiny aggregates and poor dispersion of HNTs in the PA 11 matrix, continued addition of HNTs up to 6 phr resulted in the deterioration of the thermal behavior of the nanocomposites [34]. As the HNTs content grew from 4 to 6 phr, the crystallization and melting temperatures decreased from 165.5 ℃ to 165.3 ℃ and 195.7 ℃ to 194.7 ℃, respectively. However, as HNTs content increased from 20.92% to 19.22%, the degree of crystallinity decreased. PA 11/4HNTs is the optimum number of HNTs that can be added to PA 11 nanocomposites, according to this study.
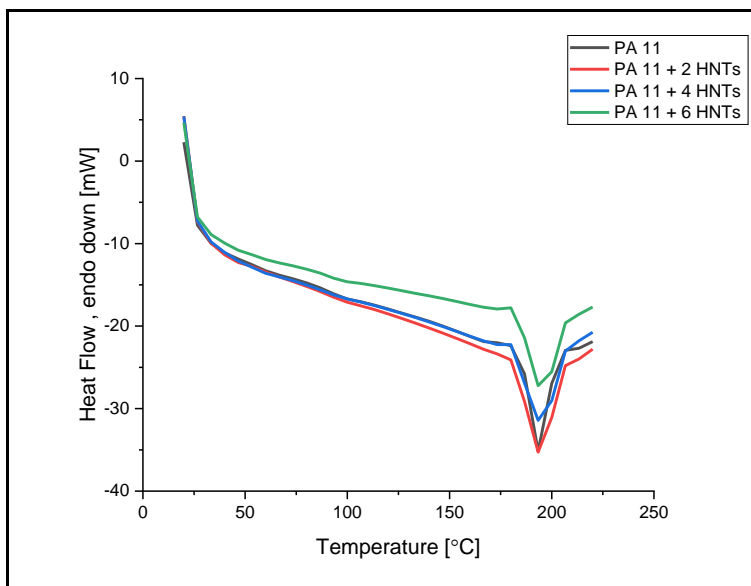

Figure 6. DSC thermograms of pure PA 11 and all PA 11 nanocomposites containing varying amounts of HNTs during heating
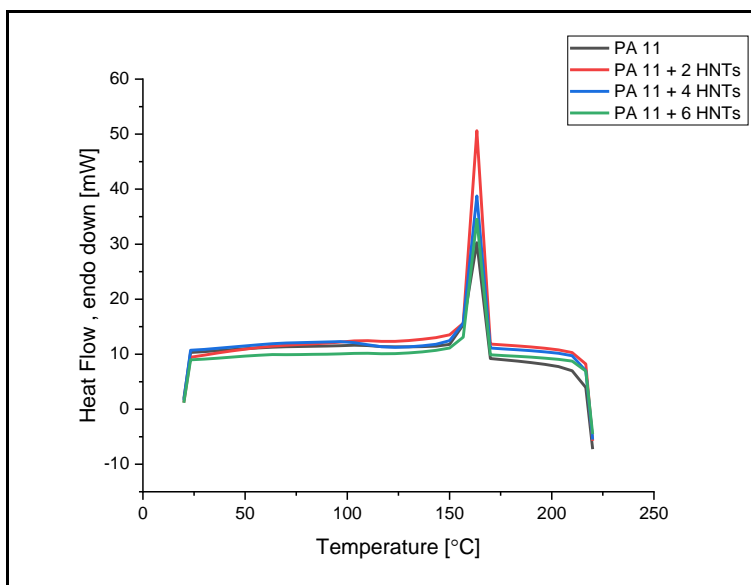

Figure 7. DSC thermograms of pure PA 11 and all PA 11 nanocomposites containing varying amounts of HNTs during cooling

Fourier Transmission Electron Microscopy
Fourier Transform Electron Microscopy
The Fourier transform infrared spectroscopy (FTIR) is an analytical technique used for identifying organic,

polymeric and inorganic materials. Test samples are scanned, and chemical characteristics are observed using infrared spectroscopy. Figure 8 depicts the FTIR spectra of pure PA 11, PA 11/2 HNTs, PA 11/4 HNTs and PA 11/6 HNTs nanocomposites to illustrate potential interactions that may occur when HNTs are introduced into PA 11. Table 4 lists and identifies the primary bands, as well as the attributions of the bands discovered.

Figure 8 shows how the sample was analyzed to determine how the functional groups differed from the pure PA 11. Peak shifting and intensity shift in the nanocomposite may show intramolecular interactions and compatibility between PA 11 and HNTs. A considerable variation may be seen in several peaks. In PA 11/2 HNTs, PA 11/4 HNTs, and PA 11/6 HNTs, there were five new peaks detected besides HNTs that emerged at 3692 cm^{-1}, 3620 cm^{-1}, 1080 cm^{-1}, 1032 cm^{-1}, and 913 cm^{-1}. The peak at 3692 cm^{-1} in the PA 11 containing HNTs nanocomposite is attributed to the hydroxyl stretching vibration of the inner surface of hydroxyl groups, whereas the peak at 3620 cm^{-1} in the nanocomposites is attributed to the O-H stretching vibration of the inner hydroxyl groups, which is between the Si-O tetrahedron and the Al-O octahedron. Peak 3692 cm^{-1} has a stronger intensity than peak 3620 cm^{-1}. The Si-O groups (Si-O-Si) and (O-Si-O) have in-plane stretching vibrations of 1080 cm^{-1}, 1078 cm^{-1}, and 1032 cm^{-1}, respectively. Finally, the peak at 912 cm^{-1} in the compounding corresponds to the inner Al-OH group O-H deformation vibration.

Cheng [35] posited a similar idea, assigning the bands at 1039 cm^{-1} and 911 cm^{-1} to Si-O stretching and deformation of the inner hydroxyl groups, respectively, whereas the O-H stretching vibrations of inner-surface Al-OH groups and inner surface Al-OH groups are at 3703 cm^{-1} and 3622 cm^{-1} respectively. The findings of Ghanbari [36] also made a similar suggestion. They claimed that including HNTs has resulted in the appearance of two new bands. The band at 1033 cm^{-1} corresponds to the Si-O-Si asymmetrical stretch vibration peak, whereas the one at 915 cm^{-1} corresponds to a single Al-OH bending band.

Table 4. Band attributions of neat PA 11

| Bands	(cm-1)	Attributions
1	3300 – 3302	N-H stretching
2	3077 – 3079	Fermi resonance (δNH amide II)
3	2918 – 2919	Asymmetric stretch of CH_2
4	2850 – 2851	Symmetrical stretch of CH_3
5	2159 – 2160	C=C stretch (alkynes)
6	2025 – 2030	
7	1634 – 1637	Amide I (C=O stretch)
8	1540 – 1542	Amide II (-NH-CO- group)
9	1466 – 1467	Bending of C=O and N- Vicinal CH_2
10	1371 – 1367	CH_3 umbrella mode
11	1276 – 1277	CH_3 stretching
12	1231 – 1232	C-H in-plane bending
13	682 – 720	CH_2 rocking
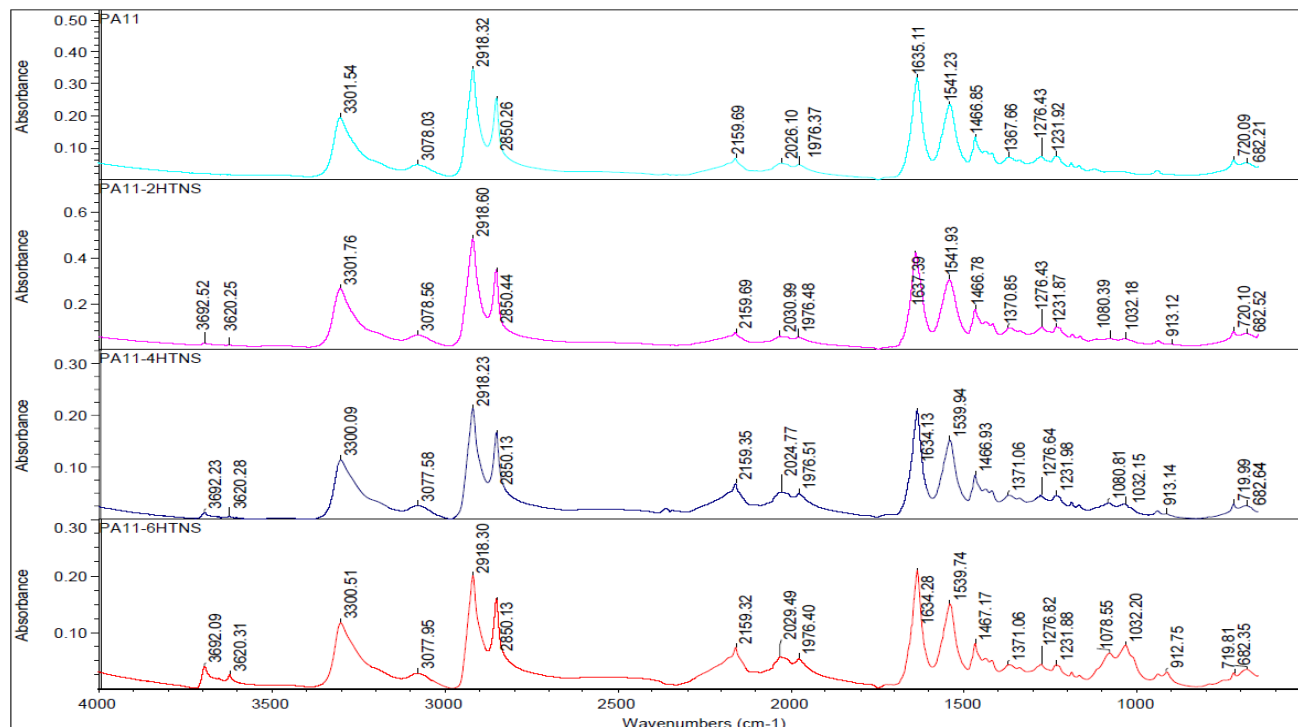
Figure 8. FTIR spectra of pure PA 11 and all PA 11 nanocomposites containing varying amounts of HNTs

Viscoelastic Properties
Dynamic Mechanical Analysis

The viscoelasticity of polymer materials was measured through Dynamic Mechanical Analysis (DMA). The DMA technique was employed in this investigation to measure the stiffness of nanocomposites at different HNTs composition, as well as the effects of HNTs composition on T_g. When examining glass transition phenomenon, DMA has a higher sensitivity than differential scanning calorimeter (DSC). DMA testing was done on the produced nanocomposites to further investigate the viscoelastic characteristics. Figure 9, Figure 10, and Figure 11 show the storage modulus, loss modulus and loss factor (tan δ) of neat PA 11 and PA 11 containing varying amounts of HNTs nanocomposites, which are reported in Table 5. Table 5 also includes the flexural modulus values of pure PA 11 and PA 11 containing varying amounts of HNTs nanocomposites for comparison with DMA results, as both tests used the same method and specimen (three-point bending method and rectangular bar specimen).

Figure 9 illustrates the storage modulus of neat PA 11 and PA 11 containing varying amount of HNTs nanocomposites as a function of temperature. When compared to pure PA 11, the storage modulus of PA 11/HNTs nanocomposites improves significantly with increasing HNTs content at room temperature (25 ℃), showing that HNTs operate as an effective reinforcing filler [10]. The reinforcement effect of high-performance HNTs combined with interfacial interactions between the polyamide 11 matrix and halloysite nanotubes fillers is ascribed to the considerable improvement in storage modulus of PA 11 containing varying amounts of HNTs nanocomposites. Incorporating HNTs into the PA 11 matrix significantly improves the material's stiffness and load-bearing capacity. These findings are in line with the flexural modulus, which increases as HNTs are added.

Figure 10 shows the loss modulus of neat PA 11 and PA 11 containing varying amount of HNTs nanocomposites as a function of temperature. The pure PA 11 has a peak temperature of 37.7 ℃, while PA11/2HNTs, PA 11/4HNTs, and PA 11/6HNTs have peak temperatures of 38.5 ℃, 38.0 ℃, and 41.5 ℃, respectively. With the addition of HNTs, the peak temperature of the loss modulus of PA 11 rises steadily. It is also worth noting that all PA 11 containing varying amounts of HNTs nanocomposites have a single peak, showing that, in the amorphous region, PA 11 and HNTs are entirely miscible.

Figure 11 shows the temperature-dependent fluctuation of the loss factor (tan δ) for pure PA 11 and PA 11 containing varying amount of HNTs nanocomposites. T_g can be determined by the peak of the tan δ. The T_g of pure PA 11 is lower than previously published values [37]. The temperature for maximal tan δ of

pure PA 11 is at 56.7 ℃, as seen in the graph. It is thought to be linked to the breakdown of hydrogen bonds between the PA 11 chain, causing long-range segmental chain movement in the amorphous area. With increasing HNTs content in the nanocomposites, the tan δ or T_g of the PA 11 containing varying amounts of HNTs nanocomposites increased from 57.7 ℃ to 58.2 ℃, which was commensurate with the trend in loss modulus. This result reflects the nanofillers' restriction of polymer chain mobility [38], as well as the HNTs effective interfacial contact with the PA 11 matrix [10].

Table 5. DMA results of pure PA 11 and all PA 11 nanocomposites containing varying amounts of HNTs

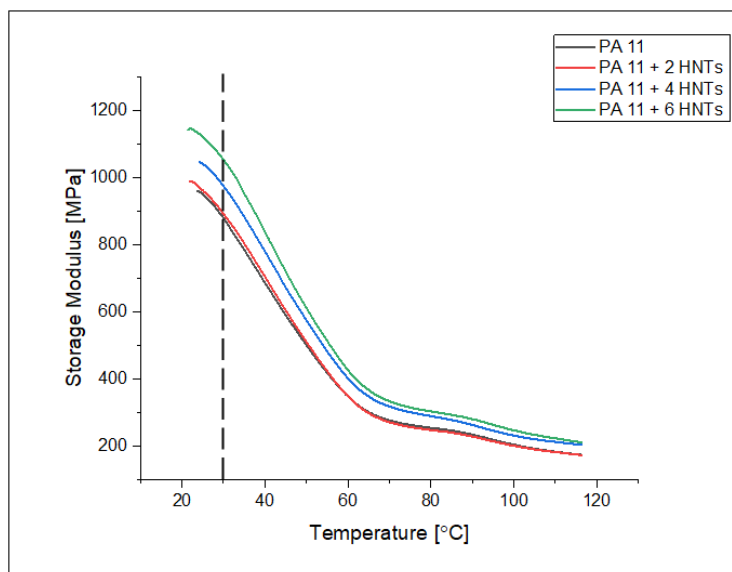| Samples	Storage Modulus at 25 ℃ (MPa)	Flexural Modulus (MPa)	Loss Modulus at peak (℃)	Tan δ at peak (℃)	Tan δ values at peak
PA 11	951	990	37.7	56.7	0.13
PA 11/2HNTs	962	1031	38.5	57.7	0.12
PA 11/4HNTs	1041	1141	38.0	57.8	0.12
PA 11/6HNTs	1122	1168	41.5	58.2	0.12

Figure 9. Storage modulus results of pure PA 11 and all PA 11 nanocomposites containing varying amounts of HNTs
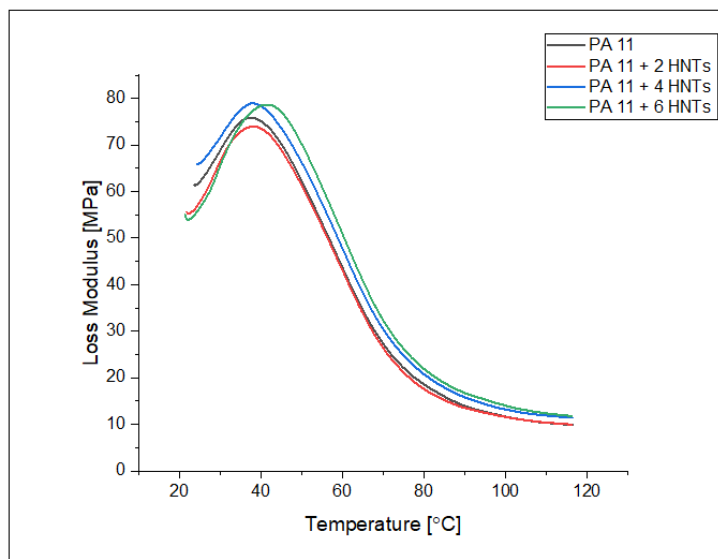
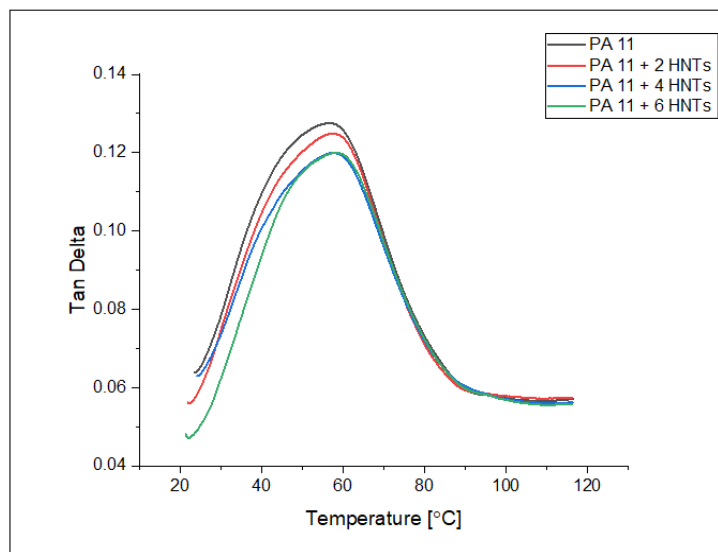**Figure 10.** Loss modulus results of pure PA 11 and all PA 11 nanocomposites containing varying amounts of HNTs.

Figure 11. Tan δ results of pure PA 11 and all PA 11 nanocomposites containing varying amounts of HNTs.

Mechanical Properties

Tensile strength

The tensile test was used to investigate the effect of HNTs loading on the mechanical properties of the PA 11 matrix. Figure 12 compares the tensile strength of the pure PA 11 matrix to all PA 11 nanocomposites containing varying amounts of HNTs. The tensile strength of pure PA 11 is 51.64 MPa. It can be shown that adding 2 and 4 phr of HNTs content increases tensile strength of PA 11, whereas adding 6 phr of HNTs content decreases tensile strength of PA 11. With the addition of 2 phr of HNTs content, the tensile strength increased to 52.72 MPa, reaching a maximum amount of 53.37 MPa with 4 phr of HNTs content. This is due to the HNTs' high dispersion in the matrix at this concentration, the nanotube reinforcing effect, and the interaction between the nanotube and the matrix. However, when the amount of HNTs in the material increased to 6 phr, the tensile strength declined to 44.52 MPa. This is because of an overabundance of HNTs, which causes nanotube aggregation as discussed in the morphology [39; 40; 41; 42].

These findings corroborate Sharif's [25] findings on the effect of HNTs on the tensile strength properties of PA 6 nanocomposites. They discovered that, when HNTs were present, the tensile strength of nanocomposites increased. This increase in tensile strength shows that HNTs operate as PA 6 reinforcing fillers. The tensile strength of the material dropped as the HNTs level increased. According to Rashmi [43], the tensile strength of PLA/PA 11 decreases with increasing HNTs content because of HNTs aggregation and lower molten compound flow during crystallinity from DSC processing.
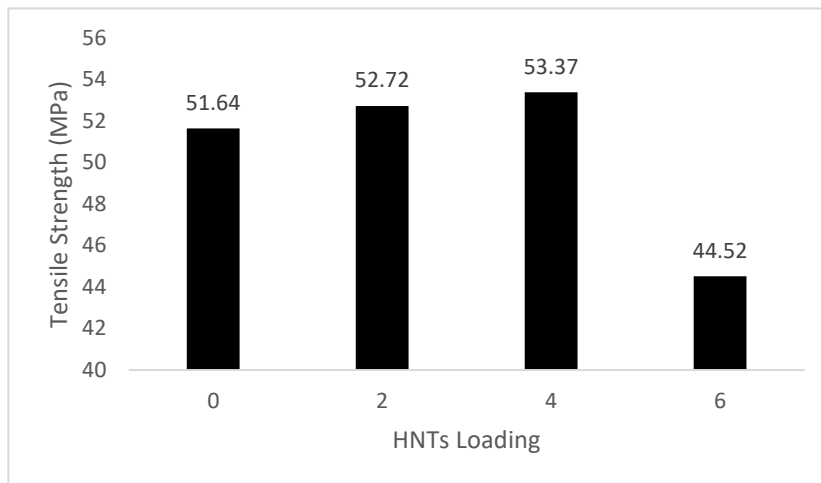
Figure 12. Tensile strength of pure PA 11 and all PA 11 nanocomposites containing varying amounts of HNTs

Young's modulus

Figure 13 depicts the Young's modulus as a function of HNTs concentration. It can be noticed that the Young's modulus of the pure PA 11 increased with the increase of HNTs loading from 0 to 6 phr. The pure PA 11 has a Young's modulus of 939.89 MPa. With the addition of 2 phr of HNTs content, the relative Young's modulus increased to 1029.46 MPa, and 1034 MPa with the addition of 4 phr of HNTs content, reaching a maximum of 1117.93 MPa at 6 phr of HNTs content. According to Bugatti [1], HNTs have been proposed to improve strength and stiffness at low concentrations due to improvements in young's modulus. The effects of HNTs on the young's modulus of PA 11 nanocomposites by melt extrusion compounding were investigated by Prashantha et al. [10; 44]. They found that raising the Young's modulus of PA 11 by 2, 4 and 6 wt.% HNTs concentration resulted in the stiffness nature of nanofillers.
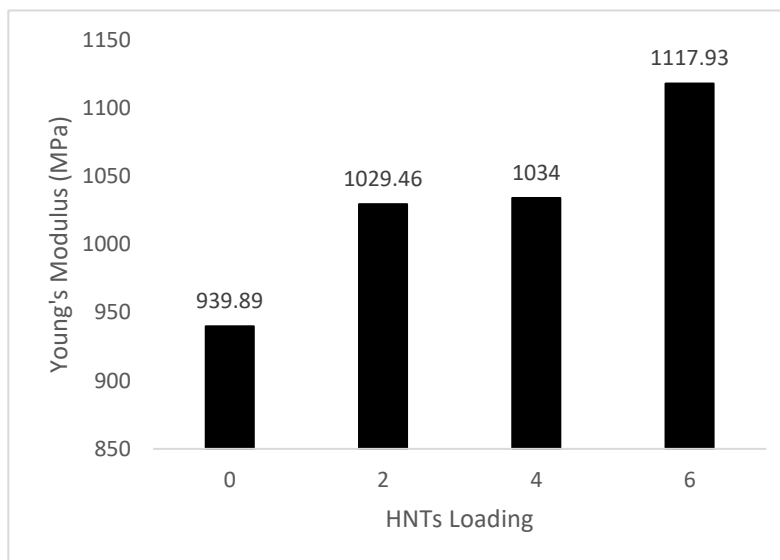
Figure 13. Young's modulus of pure PA 11 and all PA 11 nanocomposites containing varying amounts of HNTs

Elongation at break

Figure 14 depicts the effects of HNTs content on the elongation at break of PA 11 blends, revealing PA 11/2HNTs, PA 11/4HNTs and PA 11/6HNTs nanocomposites. When compared to pure PA 11 nanocomposites, adding 2 phr of HNTs content enhanced the elongation at break by roughly 1.14%. It can be shown that with an increase of 4 phr of HNTs content, the elongation at break is decreased 2.47%, while with an increase of 6 phr of HNTs content, the elongation at break is significantly decreased by 7.24%. Because the nanocomposites' crystallinity has diminished, this has occurred. By including HNTs, PA 11 nanocomposites became more brittle [45]. This trend is similar to the work of Hao [46], who investigated the influence of various loadings on the elongation at break properties of PA 11/FR/HNTs. The elongation at break of PA 11/HNTs nanocomposites improved at the lower HNTs loading of 2.5 wt.% with the presence of 15 wt.% FR and decreased at the higher HNTs loading of 10 wt.% with the presence of 25 wt.% FR, according to the researchers. These findings support Rashmi [43] findings on the effect of HNTs on the elongation at break properties of PLA/PA11 nanocomposites. They found that when 2 wt.% HNTs were present, the elongation at break of PLA/PA 11 nanocomposites increased, while when 4 wt.% and 6 wt.% HNTs were present, the elongation at break decreased. They claimed that the overloading of HNTs causes elongation at break to diminish, which can contribute to the production of aggregates or damages to PA 11 fibrils, resulting in early sample fracture.
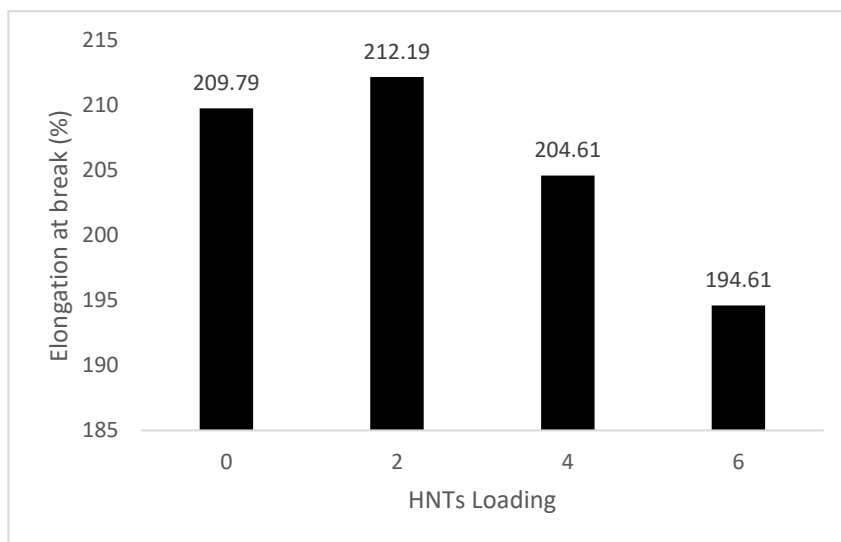

Figure 14. Elongation at break of pure PA 11 and all PA 11 nanocomposites containing varying amounts of HNTs

Flexural strength

Figure 15 depicts the influence of HNTs loading on the flexural strength of PA 11 nanocomposites. As can be seen in Figure 12, the flexural and tensile strengths of PA 11 nanocomposites with varying HNTs content follow a similar pattern. At 4 phr of HNTs, which is 12% higher than the neat blend, the ultimate peak of flexural strength appears. The increase in flexural strength is attributed to the homogenous dispersion of HNTs and a strong interfacial interaction between the HNTs and the PA 11 matrix [47]. The interfacial interaction of nanoparticles with the polymer matrix and their dispersion state in the matrix determines the reinforcing impact of nanoparticles [48]. Because flexural strength declines at this amount, the 4 phr loading of HNTs appears to be an optimal value. The value of flexural strength decreases with the addition of 6 phr of HNTs. This could be due to agglomeration of HNTs, which reduces the aspect ratio and hence reduces the contact surface between HNTs and PA 11 matrix [49; 50]. As for the maximum elastic modulus and flexibility performance of nanocomposites, Sangeetha [51] found that the linear low-density polyethylene (LLDPE)/HNTs nanocomposites improved flexural strength up to 4 phr of HNTs. Prashantha [52] made a similar observation on the influence of HNTs treatment on the structural and mechanical properties of PP nanocomposites made by a master batch technique. Including HNTs improves the flexural modulus and strength of PP, according to researchers. Flexural strength diminishes at greater loadings because overloading of HNTs causes an aggregation of the nanotube, where such micron-sized aggregates operate as weak points and failure initiation sites.
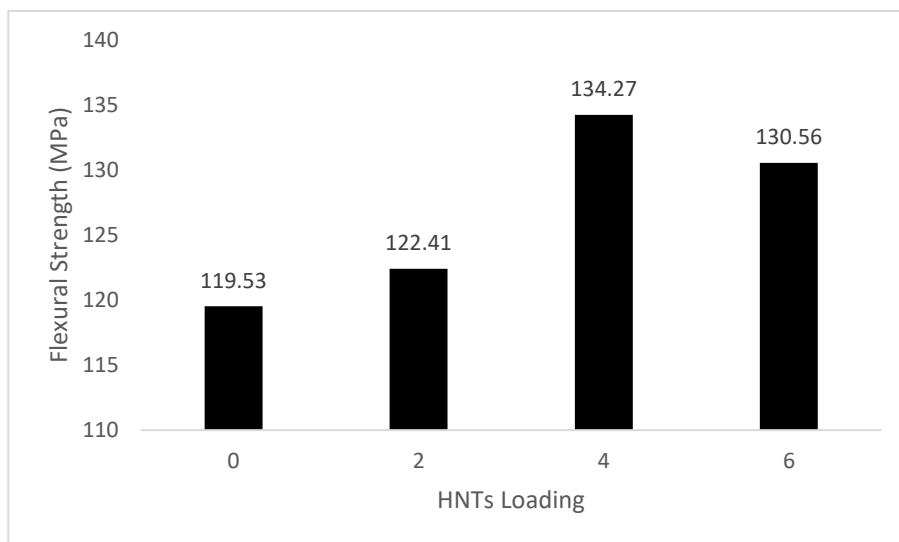
Figure 15. Flexural strength of pure PA 11 and all PA 11 nanocomposites containing varying amounts of HNTs

Flexural modulus

Figure 16 depicts the influence of HNTs powder as a filler loading on the flexural modulus of PA 11 nanocomposites. The addition of HNTs to pure PA 11 nanocomposites resulted in an increase in both flexural strength and flexural modulus value as displayed in Figure 16. The tensile modulus followed a similar pattern. Flexural modulus increased by 18.1% when 6 phr of HNTs powder is added to the PA 11 matrix. The HNTs fillers have a significant stiffening effect, and researchers have identified a similar trend in the flexural modulus properties of PA 11/HNTs nanocomposites with filler loadings of 2, 6 and 10wt.%. Incorporating inorganic HNTs increases the stiffness of nanocomposites, according to the researchers. Montava-Jorda [53] reported similar results on the mechanical characteristics of PLA/HNTs nanocomposites. They discovered that as the amount of HNTs in the PLA/HNTs nanocomposites rose, the flexural modulus of the PLA/HNTs nanocomposites increased, owing to the enhanced structural stiffness on PLA polymer chains. Moreover, Franciszczak [54] made a similar observation, claiming that adding HNTs to PP nanocomposites enhanced their flexural modulus. The filler material, its volumetric content, and shape all contribute to the increase in flexural modulus.
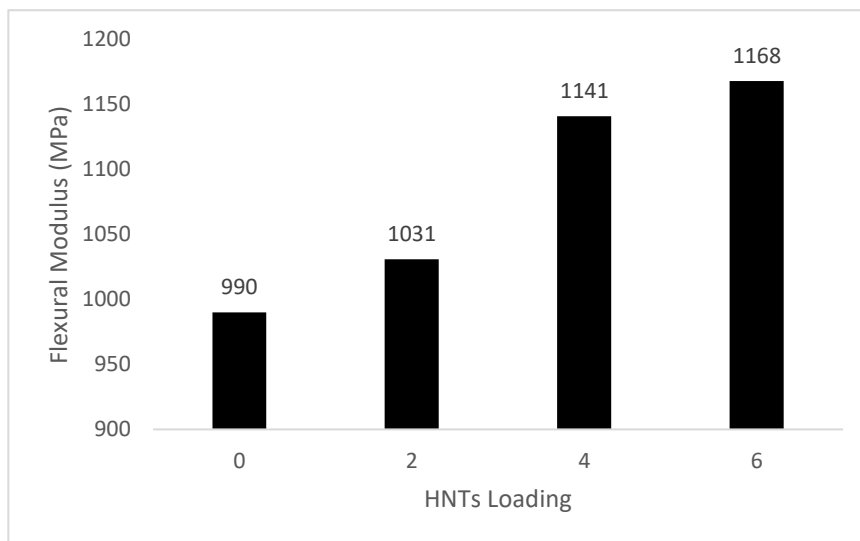

Figure 16. Flexural modulus of pure PA 11 and all PA 11 nanocomposites containing varying amounts of HNTs

Impact strength

Figure 17 depicts the effects of HNTs content as a filler loading on the Charpy impact strength of PA 11 nanocomposites. One metric that shows a material's toughness is its impact strength. With increased HNTs content, the Charpy impact strength reduced considerably. The energy density of PA 11/2HNTs nanocomposites decreased gradually from 17.10 kJ/m^2 for pure PA 11 to 13.65 kJ/m^2 for PA 11/2HNTs nanocomposites. With an increase in HNTs content, the Charpy impact strength gradually reduced. The Charpy impact strength decreases due to HNTs aggregation in the polymer matrix [42]. The influence of raw Algerian and commercial HNTs on the tribological and mechanical properties of PA 11 nanocomposites with filler loadings of 1, 3 and 5 wt.% was studied by Sahnoune [12]. The decrease in impact strength was due to the production of HNT aggregates as the HNTs content increased, acting as a stress concentrator and causing brittle failure. Jamaludin [27] found a similar observation regarding PET/PC compatibility with HNTs. The impact strength was reduced as expected because of the production of HNTs aggregates with increasing content, which act as a stress concentrator to induce brittle failure.
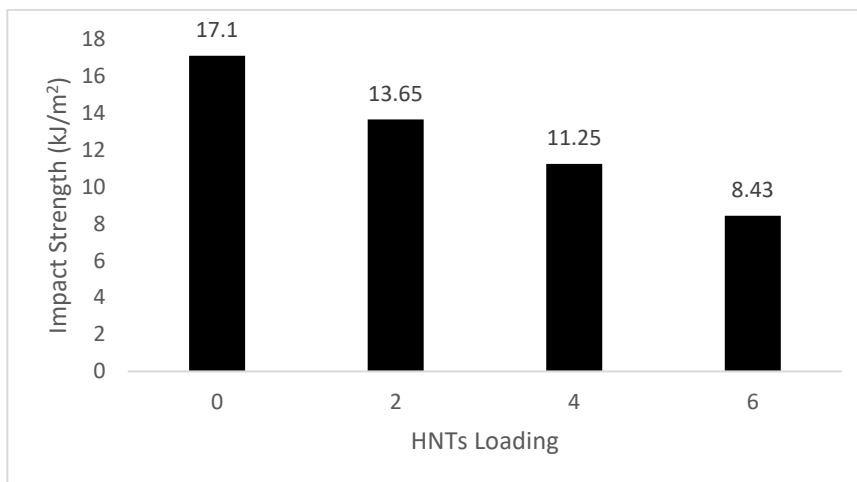

Figure 17. The impact strength of pure PA 11 and all PA 11 nanocomposites containing varying amounts of HNTs

Flammability properties

UL-94 Flammability

To determine the self-extinguishing behavior and burning rate of PA 11 nanocomposites containing varying amounts of HNTs developed compared to pure PA 11, vertical and horizontal UL-94 burning tests were conducted. According to the ASTM D5048 standard, the pure PA 11, PA 11/2HNTs, PA 11/4HNTs and PA 11/6HNTs nanocomposites were subjected to the UL-94 horizontal burning test. Table 6 shows a summary of the findings. This test is used to assess a material's HB flammability rating. There was no charring at the surface of the pure PA 11 and PA 11 nanocomposites containing varying amounts of HNTs content, which were burnt with drips. However, for the pure PA 11 and PA 11 nanocomposites with varying HNTs, the burning rate could be calculated because none of the specimens examined for each composition burned for long enough to meet the standard's requirements. In the HB test, the time taken for the flame front to reach the 25 mm mark for pure PA 11 was 3.8 seconds; however, the time taken for the flame front to reach the 25 mm mark increased to 4.2, 4.8 and 4.4 seconds for the PA 11 nanocomposites containing varying amounts of HNTs. The addition of HNTs to the polymer matrix caused the nanocomposites to self-extinguish, showing that they might be assessed using the vertical burning test, which analyzes such behaviors. By swiftly extinguishing the flame before the first mark, all nanocomposite compositions pass the UL-94 HB rating.

The UL-94 vertical burning test was also done on all samples according to the ASTM D3801 standard to further study the ignitability and flammability of the pure PA 11 and all PA 11 nanocomposites containing varying amounts of HNTs. The mean after-flame periods (t_1 and t_2) are shown in Table 7, along with some qualitative information from test observations and material evaluations. In the UL-94 vertical burning test, pure PA 11 and all PA 11 nanocomposites containing varying amounts of HNTs self-extinguished the flame. For both pure PA 11 and all PA 11 nanocomposites containing varying amounts of HNTs, no afterglow period was recorded, and none of them burnt up to the holding clamp.

This trend was not found in the current study. All PA 11 nanocomposites containing varying amounts of HNTs exhibited after-flame timings (t_1 and t_2) and all of them, including pure PA 11, were classified as V-

2. The nanocomposites were not granted a higher rating because they all had self-extinguishing properties and flame dripping during the combustion process, which burned the cotton underneath the sample [55]. Butler [56] used HNTs and a standard intumescent to create a better PA 11 composite with improved mechanical, thermal, and flammability qualities. They found that without including FR additives, none of the PA 11/HNTs nanocomposites (2.5, 5, 7.5, and 10 wt.%) could attain an UL-94 V-0 grade.

Table 6. Horizontal burning test results in accordance with UL-94 for pure PA 11 and all PA 11 nanocomposites containing varying amounts of HNTs

Horizontal Flame Testing						
Samples	Time for flame front to reach 25 mm mark (sec)	Time for flame front to reach 100 mm mark (sec)	If 100 mm mark not reached		Burning rate (mm/minute)	Remarks
			Time for flaming to cease (sec)	Distance flame reached from 25 mm mark (mm)		
PA 11	3.8	N/A	N/A	N/A	HB	Not burn
PA 11/2HNTs	4.2	N/A	N/A	N/A	HB	Not burn
PA 11/4HNTs	4.8	N/A	N/A	N/A	HB	Not burn
PA 11/6HNTs	4.4	N/A	N/A	N/A	HB	Not burn

*N/A= not applicable

Table 7. Vertical burning test results in accordance with UL-94 for pure PA 11 and all PA 11 nanocomposites containing varying amounts of HNTs

Vertical Flame Testing					
Samples	Sample burning time after first flame application (sec)	Sample burning time after second flame application (sec)	Flaming Drip	Rating	Remarks
PA 11	28.2	9.8	Yes	V-2	Partially burn
PA 11/2HNTs	26.2	22.2	Yes	V-2	Partially burn
PA 11/4HNTs	16.1	23.3	Yes	V-2	Partially burn
PA 11/6HNTs	24.4	8.2	Yes	V-2	Partially burn

Conclusions

This study revealed that the tensile and flexural strength of PA 11 matrix were generally improved with incorporation of HNTs with maximum value recorded at 4 phr. However, the tensile and flexural modulus of PA 11 nanocomposites were found to increase with increasing of HNTs content up to 6 phr. The maximum improvement in elongation at break was observed at 2 phr of HNTs. The impact strength decreased as the percentage of HNTs increase. The DSC showed a steady increase in melting temperature (T_m) as HNTs content increase up to 4 phr while the crystallization temperature (T_c) remained unchanged, and it was higher than the neat PA 11 nanocomposites. A single T_g was observed for PA 11/HNTs nanocomposites in DMA analysis, and it was higher than the T_g of neat PA 11 nanocomposites due to the improved interfacial adhesion between the phases and a better dispersion of HNTs in the PA 11 matrix. The thermal stability of PA 11 nanocomposites was highest for the sample containing 4 phr HNTs. SEM revealed that HNTs are distributed and homogenously dispersed with incorporation of 2 and 4 phr of HNTs while it starts HNTs aggregates when 6 phr of HNTs was added. For all formulations, the flammability characteristics of PA 11 and PA 11/HNTs nanocomposites in their natural state exhibit a HB and V-2 rate. The improvement in the properties of PA 11/HNTs was attributed to the improved interfacial adhesion between all phases resulting from the interaction of hydrogen bonding between PA 11 and HNTs. FTIR analysis indicated such interactions. The developed HNTs reinforced PA 11 nanocomposites have potential applications in the automotive and selective laser sintering (SLS) industry where the thermal stability with balanced strength, stiffness and toughness properties are required.

Conflicts of Interest

The author(s) declare(s) that there is no conflict of interest regarding the publication of this paper.

Acknowledgment

References

[1]   V. Bugatti, L. Vertuccio, G. Viscusi, and G. Gorrasi. (2018). Antimicrobial membranes of bio-based pa 11 and hnts filled with lysozyme obtained by an electrospinning process. *Nanomaterials*, *8*(3). Doi: 10.3390/nano8030139.

[2]   R. Androsch, K. Jariyavidyanont, and C. Schick. (2019). Enthalpy relaxation of polyamide 11 of different morphology far below the glass transition temperature. *Entropy*, *21*(10), 984. Doi: 10.3390/e21100984.

[3]   S. Fu, Z. Sun, P. Huang, Y. Li, and N. Hu. (2019). Some basic aspects of polymer nanocomposites: A critical review. *Nano Mater. Sci.*, *1*(1), 2-30. Doi: 10.1016/j.nanoms.2019.02.006.

[4]   H. C. Bidsorkhi, H. Adelnia, R. Heidar Pour, and M. Soheilmoghaddam. (2015). Preparation and characterization of ethylene-vinyl acetate/halloysite nanotube nanocomposites. *J. Mater. Sci.*, *50*(8), 3237-3245. Doi: 10.1007/s10853-015-8891-6.

[5]   M. Mousa and Y. Dong. (2021). *Multiscaled PVA Bionanocomposite Films*.

[6]   C. L. Ng and W. S. Chow. (2020). Multifunctional halloysite nanotube–reinforced polypropylene/polyamide binary nanocomposites. *Polym. Polym. Compos.*, *28*(8-9), 623-630. Doi: 10.1177/0967391119895441.

[7]   N. Arman, E. Tekay, and S. Şen. (2020). Preparation of high-strength SEBS nanocomposites reinforced with halloysite nanotube: Effect of SEBS-g-MA compatibilizer. *J. Thermoplast. Compos. Mater.*, *33*(10), 1336-1357. Doi: 10.1177/0892705719895055.

[8]   D. Marset *et al.* (2020). The effect of halloysite nanotubes on the fire retardancy properties of partially biobased polyamide 610. *Polymers (Basel).*, *12*(12), 1-21. Doi: 10.3390/polym12123050.

[9]   Z. Kovačević, S. Flinčec Grgac, and S. Bischof. (2021). Progress in biodegradable flame retardant nano-biocomposites. *Polymers (Basel).*, *13*(5), 1-30. Doi: 10.3390/polym13050741.

[10]   K. Prashantha, M. F. Lacrampe, and P. Krawczak. (2013). Highly dispersed polyamide-11/halloysite nanocomposites: Thermal, rheological, optical, dielectric, and mechanical properties. *J. Appl. Polym. Sci.*, *130*(1), 313-321. Doi: 10.1002/app.39160.

[11]   D. Francisco, L. de Paiva, W. Aldeia, A. Lugao, and E. Moura. (2019). *Investigation on mechanical behaviors of polyamide 11 reinforced with halloysite nanotubes*. Springer International Publishing. 693-701. Doi: 10.1007/978-3-030-05749-7_69.

[12]   M. Sahnoune *et al.* (2019). Tribological and mechanical properties of polyamide-11/halloysite nanotube nanocomposites. *J. Polym. Eng.*, *39*(1), 25-34. Doi: 10.1515/polyeng-2018-0131.

[13]   M. Sahnoune, M. Kaci, H. Garay, J. M. Lopez-Cuesta, and M. Mahlous. (2021). Effects of gamma irradiation on structural, thermal and mechanical properties of polyamide-11/halloysite nanotubes nanocomposites. *J. Thermoplast. Compos. Mater.* Doi: 10.1177/08927057211031966.

[14]   Y. Dong and D. Bhattacharyya. (2008). Effects of clay type, clay/compatibiliser content and matrix viscosity on the mechanical properties of polypropylene/organoclay nanocomposites. *Compos. Part A Appl. Sci. Manuf.*, *39*(7), 1177-1191. Doi: 10.1016/j.compositesa.2008.03.006.

[15]   K. Fukushima, D. Tabuani, and G. Camino. (2009). Nanocomposites of PLA and PCL based on montmorillonite and sepiolite. *Materials Science and Engineering C*, *29*(4), 1433-1441. Doi: 10.1016/j.msec.2008.11.005.

[16]   E. Girard, X. Liu, J. D. Marty, and M. Destarac. (2014). RAFT/MADIX (co)polymerization of vinyl trifluoroacetate: A means to many ends. *Polym. Chem.*, *5*(3), 1013-1022. Doi: 10.1039/c3py01109g.

[17]   I. Kolesov *et al.* (2013). Crystallization of a polyamide 11/organo-modified montmorillonite nanocomposite at rapid cooling. *Colloid Polym. Sci.*, *291*(11), 2541-2549. Doi: 10.1007/s00396-013-2977-y.

[18]   M. Sahnoune *et al.* (2020). Effects of functionalized halloysite on morphology and properties of polyamide-11 / SEBS-g-MA blends To cite this version : HAL Id : hal-02892647.

[19]   N. B. A. Thompson *et al.* (2021). The thermal decomposition of studtite: analysis of the amorphous phase. *J. Radioanal. Nucl. Chem.*, *327*(3), 1335-1347. Doi: 10.1007/s10967-021-07611-4.

[20]   S. Zhang, Q. Ran, X. Zhang, and Y. Gu. (2021). Effects of the curing atmosphere on the structures and properties of polybenzoxazine films. *J. Mater. Sci.*, *56*(3), 2748-2762. Doi: 10.1007/s10853-020-05425-5.

[21]   P. Loulergue, M. Amela-Cortes, S. Cordier, Y. Molard, L. Lemiègre, and J. L. Audic. (2017). Polyurethanes prepared from cyclocarbonated broccoli seed oil (PUcc): New biobased organic matrices for incorporation of phosphorescent metal nanocluster. *J. Appl. Polym. Sci.*, *134*(45), 1-10. Doi: 10.1002/app.45339.

[22]   A. Jumahat, A. A. A. Talib, and A. Abdullah. (2016). *Wear Properties of Nanoclay Filled Epoxy Polymers and Fiber Reinforced Hybrid Composites*.

[23]   R. Crossley, P. Schubel, and A. Stevenson. (2014). Furan matrix and flax fibre as a sustainable renewable composite: Mechanical and fire-resistant properties in comparison to phenol, epoxy and polyester. *J. Reinf. Plast. Compos.*, *33*(1), 58-68. Doi: 10.1177/0731684413502108.

[24]   J. H. Wu, C. W. Chen, M. C. Kuo, M. S. Yen, and K. Y. Lee. (2018). High toughness and fast crystallization poly(lactic acid)/polyamide 11/SiO₂ composites. *J. Polym. Environ.*, *26*(2), 626-635. Doi: 10.1007/s10924-017-0977-6.

[25]   N. F. A. Sharif, Z. Mohamad, A. Hassan, and M. U. Wahit. (2012). Novel epoxidized natural rubber toughened polyamide 6/halloysite nanotubes nanocomposites. *J. Polym. Res.*, *19*(1). Doi: 10.1007/s10965-011-9749-5.

[26]   J. Arshad, N. K. Janjua, and R. Raza. (2021). Synthesis of novel (Be,Mg,Ca,Sr,Zn,Ni)3O4 high entropy oxide with characterization of structural and functional properties and electrochemical applications. *J. Electrochem. Sci. Technol.*, *12*(1), 112-125. Doi: 10.33961/jecst.2020.01130.

[27]   N. A. Jamaludin, I. M. Inuwa, A. Hassan, N. Othman, and M. Jawaid. (2015). Mechanical and thermal properties of SEBS-g-MA compatibilized halloysite nanotubes reinforced polyethylene terephthalate/polycarbonate/nanocomposites. *J. Appl. Polym. Sci.*, *132*(39), 1-10. Doi: 10.1002/app.42608.

[28]   M. Mrówka, A. Woźniak, J. Nowak, G. Wróbel, and S. Sławski. (2021). Determination of mechanical and tribological properties of silicone-based composites filled with manganese waste," *Materials (Basel).*, *14*(16). Doi: 10.3390/ma14164459.

[29]   L. Mancic, R. F. M. Osman, A. M. L. M. Costa, J. R. M. d'Almeida, B. A. Marinkovic, and F. C. Rizzo. (2015). Thermal and mechanical properties of polyamide 11 based composites reinforced with surface modified titanate nanotubes. *Mater. Des.*, *83*(459-467). Doi: 10.1016/j.matdes.2015.06.059.

[30]   D. Carponcin *et al.* (2014). Discontinuity of physical properties of carbon nanotube/polymer composites at the percolation threshold. *J. Non. Cryst. Solids*, 392-393, 19-25. Doi: 10.1016/j.jnoncrysol.2014.03.022.

[31]   A. Zubkiewicz, A. Szymczyk, S. Paszkiewicz, R. Jędrzejewski, E. Piesowicz, and J. Siemiński. (2020). Ethylene vinyl acetate copolymer/halloysite nanotubes nanocomposites with enhanced mechanical and thermal properties. *J. Appl. Polym. Sci.*, *137*(38), 1-12. Doi: 10.1002/app.49135.

[32]   N. A. Jamaludin, A. Hassan, N. Othman, and M. Jawaid. (2015). Effects of halloysite nanotubes on mechanical and thermal stability of poly(ethylene terephthalate)/polycarbonate nanocomposites. *Appl. Mech. Mater.*, 735, 8-12. Doi: 10.4028/www.scientific.net/amm.735.8.

[33]   I. M. Inuwa, T. B. Keat, and A. Hassan. (2016). Mechanical and thermal properties of hybrid Graphene/Halloysite nanotubes reinforced polyethylene terepthalate nanocomposites. *Nanoclay Reinf. Polym. Compos.* Springer, Singapore. 309-327. Doi: 10.1007/978-981-10-1953-1.

[34]   S. Rojas-Lema, L. Quiles-Carrillo, D. Garcia-Garcia, B. Melendez-Rodriguez, R. Balart, and S. Torres-Giner. (2020). Tailoring the properties of thermo-compressed polylactide films for food packaging applications by individual and combined additions of lactic acid oligomer and halloysite nanotubes. *Molecules*, *25*(8), 1-23. Doi: 10.3390/molecules25081976.

[35]   Z.-L. Cheng, X.-Y. Chang, Z. Liu, and D.-Z. Qin. (2018). Surface-modified halloysite nanotubes as fillers applied in reinforcing the performance of polytetrafluoroethylene. *Clay Miner.*, *53*(4), 643-656. Doi: 10.1180/clm.2018.48.

[36]   M. Ghanbari, D. Emadzadeh, W. J. Lau, H. Riazi, D. Almasi, and A. F. Ismail. (2016). Minimizing structural parameter of thin film composite forward osmosis membranes using polysulfone/halloysite nanotubes as membrane substrates. *Desalination*, *377*, 152-162. Doi: 10.1016/j.desal.2015.09.019.

[37]   T. X. Liu, D. Chen, I. Y. Phang, and C. Wei. (2014). Studies on crystal transition of polyamide 11 nanocomposites by variable-temperature x-ray diffraction. *Chinese J. Polym. Sci. (English Ed.)*, *32*(1), 115-122. Doi: 10.1007/s10118-014-1383-3.

[38]   R. Krishnamoorti, R. A. Vaia, and E. P. Giannelis. (1996). Structure and dynamics of polymer-layered silicate nanocomposites. *Chem. Mater.*, *8*, 1728-1734. Doi: 10.1021/cm960127g.

[39]   D. Rawtani and Y. K. Agrawal. (2012). Multifarious applications of halloysite nanotubes: A review. *Rev. Adv. Mater. Sci.*, *30*(3), 282-295.

[40]   M. Liu, B. Guo, M. Du, X. Cai, and D. Jia. (2007). Properties of halloysite nanotube-epoxy resin hybrids and the interfacial reactions in the systems. *Nanotechnology*, *18*(45). Doi: 10.1088/0957-4484/18/45/455703.

[41]   M. Du and D. Jia. (2009). Newly emerging applications of halloysite nanotubes : a review. June, 574-582. Doi: 10.1002/pi.2754.

[42]   N. K. Mohamed, V. Kochkodan, A. Zekri, and S. Ahzi. (2020). Polysulfone membranes embedded with halloysites nanotubes: Preparation and properties. *Membranes (Basel).*, *10*(1). Doi: 10.3390/membranes10010002.

[43]   B. J. Rashmi, K. Prashantha, M. F. Lacrampe, and P. Krawczak. (2015). Toughening of poly(Lactic acid) without sacrificing stiffness and strength by melt-blending with polyamide 11 and selective localization of halloysite nanotubes. *Express Polym. Lett.*, *9*(8), 721-735. Doi: 10.3144/expresspolymlett.2015.67.

[44]   K. Prashantha, H. Schmitt, M. F. Lacrampe, and P. Krawczak. (2011). Mechanical behaviour and essential work of fracture of halloysite nanotubes filled polyamide 6 nanocomposites. *Compos. Sci. Technol.*, *71*(16), 1859-1866. Doi: 10.1016/j.compscitech.2011.08.019.

[45]   S. Thanakkasaranee, K. Sadeghi, and J. Seo. (2020). Smart steam release of newly developed temperature-responsive nanocomposite films derived from phase change material. *Polymer (Guildf).*, *219*(November), 123543. Doi: 10.1016/j.polymer.2021.123543.

[46]   A. Hao *et al.* (2014). *Mechanical, thermal, and flame-retardant performance of polyamide 11 – halloysite nanotube nanocomposites.* 157-167. Doi: 10.1007/s10853-014-8575-7.

[47]   K. Szpilska, K. Czaja, and S. Kudła. (2015). Halloysite nanotubes as polyolefin fillers. *Polimery/Polymers.* *60*(6), 359-371. Doi: 10.14314/polimery.2015.359.

[48]   H. S. Khare and D. L. Burris. (2010). A quantitative method for measuring nanocomposite dispersion. *Polymer (Guildf).*, *51*(3), 719-729. Doi: 10.1016/j.polymer.2009.12.031.

[49]   S. Deng, J. Zhang, and L. Ye. (2009). Halloysite-epoxy nanocomposites with improved particle dispersion through ball mill homogenisation and chemical treatments. *Compos. Sci. Technol.*, *69*(14), 2497-2505. Doi: 10.1016/j.compscitech.2009.07.001.

[50]   G. Mishra and M. Mukhopadhyay. (2018). Enhanced antifouling performance of halloysite nanotubes (HNTs) blended poly(vinyl chloride) (PVC/HNTs) ultrafiltration membranes: For water treatment. *J. Ind. Eng. Chem.*, *63*, 366-379. Doi: 10.1016/j.jiec.2018.02.037.

[51]   V. Sangeetha, D. Gopinath, R. Prithivirajan, V. Girish Chandran, and R. Manoj Kumar. 2020. Investigating the

mechanical, thermal and melt flow index properties of HNTs – LLDPE nano composites for the applications of rotational moulding. *Polym. Test. 89*, 106595. Doi: 10.1016/j.polymertesting.2020.106595.

[52]   K. Prashantha, M. F. Lacrampe, and P. Krawczak. (2011). Processing and characterization of halloysite nanotubes filled polypropylene nanocomposites based on a masterbatch route: Effect of halloysites treatment on structural and mechanical properties. *Express Polym. Lett.*, *5*(4), 295-307. Doi: 10.3144/expresspolymlett.2011.30.

[53]   S. Montava-Jorda, V. Chacon, D. Lascano, L. Sanchez-Nacher, and N. Montanes. (2019). Manufacturing and characterization of functionalized aliphatic polyester from poly(lactic acid) with halloysite nanotubes. *Polymers (Basel).*, *11*(8), Doi: 10.3390/polym11081314.

[54]   P. Franciszczak, I. Taraghi, S. Paszkiewicz, A. Meljon, E. Piesowicz, and M. Burzyński. (2020). Effect of halloysite nanotube on mechanical properties, thermal stability and morphology of polypropylene and polypropylene/short kenaf fibers hybrid biocomposites. *Materials (Basel).*, *13*(19), 1-13. Doi: 10.3390/ma13194459.

[55]   H. Wu, R. Ortiz, and J. H. Koo. (2018). Rubber toughened flame retardant (FR) polyamide 11 nanocomposites Part 1: the effect of SEBS-g-MA elastomer and nanoclay. *Flame Retard. Therm. Stab. Mater.*, *1*(1), 25-38. Doi: 10.1515/flret-2018-0003.

[56]   S. Butler, G. Kim, J. H. Koo. (2011). Polyamide 11-Halloysite nanotube nanocomposites: Mechanical, thermal and flammability characterization. *Proceedings of the 2011, SAMPE ISTC.*